Tellus (1992), *44A*, 236–251

The diagnosis of a pre-blocking explosively-developing extratropical cyclone system

By MARY A. UHL, PHILLIP J. SMITH and ANTHONY R. LUPO, *Department of Earth and Atmospheric Sciences, Purdue University, West Lafayette, IN 47907 USA*, and PETER ZWACK, *Department of Physics, University of Quebec at Montreal, Montreal, Quebec, Canada H3C 3P8*

(Manuscript received 17 April 1991; in final form 5 November 1991)

ABSTRACT

This paper presents the diagnosis of an extratropical cyclone that developed explosively from 18 to 19 January 1979 over the North Atlantic Ocean. The diagnosis applies data obtained from the Goddard Laboratory for Atmospheres FGGE SOP-1 level III-b global analyses on a 4° latitude by 5° longitude grid to the extended height tendency and the Zwack-Okossi development equations. The cyclone developed initially in response to cyclonic vorticity advection downstream from an upper air trough, warm air advection in a strongly baroclinic region, and latent heat release in the cyclone domain. As development continued, thermal advection and latent heat release increased their role in forcing height falls in the cyclone domain, while the influence of vorticity advection decreased. Finally, development ceased when anticyclonic vorticity advection below 700 mb and adiabatic cooling in the ascending air combined to neutralize the influence of warm air advection and latent heat release.

1. Introduction

Few aspects of large-scale atmospheric dynamics have attracted the interest of the meteorological community more than has the study of extra-tropical cyclones. With circulations generally classified as synoptic scale, these cyclones interact with both larger and smaller scale circulations; harbor jet stream flows; stimulate cloud and precipitation events; lead to major wind and temperature changes; and, in short, along with their anticyclonic partners, cause many of the day-to-day extratropical weather changes. Over the last several years special interest has developed in the sub-class of extratropical cyclones that are observed to develop explosively. Referred to as "bombs" by Sanders and Gyakum (1980), such cyclones exhibit decreases in central pressure greater than or equal to 1 Bergeron, defined as 24 mb/24 h multiplied by the latitude adjustment factor $\sin \phi / \sin 60°$, where ϕ is the latitude of the cyclone center midway through the explosive development period.

Sanders and Gyakum's (1980) climatology of the bomb shows explosive cyclogenesis to be a largely maritime, cold season event occurring within or poleward of maximum westerlies and within or ahead of planetary scale troughs. Most occur approximately 500 km downstream from a mobile 500 mb trough, near a strong sea surface temperature gradient. Sanders (1986) describes a region of high frequency for explosive cyclogenesis as being over the Atlantic Ocean, northeastward from east of the Carolinas to south of Newfoundland, with storm tracks concentrating along the Gulf Stream in the winter. Gyakum et al.'s (1989) Pacific climatology shows the storm tracks within or northward of the Kuroshio current. Davis and Emanuel (1988) more generally cite the western ocean regions, where sea surface temperatures are greatest for a given latitude, as areas likely for explosive cyclogenesis.

In an attempt to gain insight into the cause of explosive deepening, attention has focused on several factors contributing to the development of these essentially baroclinic disturbances, including the influences of latent heat release, sensible heat transfer, temperature advection, static stability, upper level forcing and lower level structure (e.g., Sanders and Gyakum, 1980; Anthes et al., 1983;

Bosart and Lin, 1984; Uccellini et al., 1985; Sanders, 1986; Reed and Albright, 1986; Tsou et al., 1987; Nuss and Anthes, 1987; Davis and Emanuel, 1988; Reed et al., 1988; Kuo and Reed, 1988; Wash et al., 1988; Elsberry and Kirchoffer, 1988; MacDonald and Reiter, 1988; Roebber, 1989; Manobianco, 1988a, b; Hirschberg and Fritsch, 1991). From these, one realizes that no single process can be identified as the primary causative factor in determining whether a given cyclone will deepen explosively. Rather, as suggested by Uccellini et al. (1987) and Davis and Emanuel (1988), an interaction of several dynamic and diabatic mechanisms is likely, with each process necessary for explosive development, but no one process sufficient to singularly cause it.

Among the important roles that intense, extratropical cyclone systems play is their influence on the subsequent development of downstream blocking ridges. Studies by Green (1977), Austin (1980), Hansen and Chen (1982), Shutts (1983), Illari (1984), Mullen (1987), Colucci (1985, 1987), and Hayashi and Golder (1987) indicate that blocking can often be associated with thermal and vorticity transports induced by upstream cyclone systems and with interactions between the cyclone scale and larger scales. In two recent papers Tsou and Smith (1990a, b) found that a case of 500 mb blocking centered over southern Greenland was dynamically linked to a cyclone system that developed explosively off the east coast of North America 36 to 60 h prior to the first appearance of closed anticyclonic circulation. The forcing of the anticyclone was attributed to anticyclonic vorticity advection that developed on the anticyclonic side of a jet streak that formed east of the fully-developed upper air low 12 h prior to the first anticyclone appearance. While interaction with the downstream block was established, little was said about the forcing of the cyclone itself. The present paper completes the diagnosis by documenting the explosive development of the pre-blocking cyclone system.

2. Data and methodology

The analyzed fields used for this case study are from the First Special Observing Period (SOP-1) of the First GARP Global Experiment (FGGE) level III-b global analyses provided by the Goddard Laboratory for Atmospheres (GLA). The analysis scheme is a modification of the Cressman (1959) scheme based on the method of Bergthorsson and Doos (1955) but includes variable data density and quality. The assimilation/forecast model used is the global fourth-order version of the GLA General Circulation Model (GCM) described by Kalnay-Rivas et al. (1977) and Kalnay-Rivas and Hoitsma (1979). The model has nine sigma layers vertically and a 4° latitude by 5° longitude horizontal grid. Analyses presented in the next section show that this resolution is sufficient to depict the synoptic-scale features representative of the developing cyclone system.

Eastward and northward wind components, geopotential height, and relative humidity are analyzed at mandatory pressure levels, while surface pressure and temperature are reduced to sea level and analyzed. The analyzed data are then compared with model first-guess fields interpolated from sigma levels. After this comparison, analyzed data that differ significantly from the model first-guess are labeled as suspect, rechecked and then rejected if the difference from the model first-guess differs from the average of the nearby differences by more than set limits described in Baker (1983, Table 2). To reduce the error introduced by vertical interpolation from pressure levels to sigma levels, differences between model first-guess and analyzed fields are interpolated back to sigma levels. New initialized sigma fields for the next 6 h model forecast are the sum of the original model fields and the difference between the analyzed data and the model first-guess fields. A detailed description of this data manipulation can be found in Baker (1983).

This study used only the portion of the original data set extending from 0° to 120°W and 22° to 82°N. Within this domain the cyclone system was diagnosed from 1200 GMT 18 January to 1200 GMT 19 January 1979, its explosive development period. Mandatory level data were interpolated or extrapolated to standard isobaric surfaces from 1050 mb to 50 mb increments, using the vertical interpolation technique described in Baker (1983) in order to be consistent with original data manipulation.

The basic diagnostic tool used in this study was the extended height tendency equation described

by Tsou et al. (1987). With a frictional term added, this equation becomes

$$\left[\nabla^2+\frac{(\zeta+f)f}{\sigma}\frac{\partial^2}{\partial p^2}\right]\frac{\partial\phi}{\partial t}$$

$$=-f\boldsymbol{V}\cdot\nabla(\zeta+f)+\frac{(\zeta+f)f}{\sigma}R\frac{\partial}{\partial p}\left(\boldsymbol{V}\cdot\nabla\frac{T}{p}\right)$$

(A) (B)

$$-\frac{(\zeta+f)f}{\sigma}\frac{R}{c_p}\frac{\partial}{\partial p}\left(\frac{\dot{q}}{p}\right)-\frac{(\zeta+f)f}{\sigma}\omega\frac{\partial\sigma}{\partial p}+f\boldsymbol{k}\cdot\nabla\times\boldsymbol{F},$$

(C) (D) (E)

(1)

where σ is the static stability parameter $-RT/p\theta$ $(\partial\theta/\partial p)$; ζ the vertical component of relative vorticity; f the coriolis parameters; $\boldsymbol{V}$ the horizontal wind vector; ω the vertical motion in isobaric coordinates $(\mathrm{d}p/\mathrm{d}t)$; $\boldsymbol{F}$ the frictional force; q the diabatic heating rate per unit mass; ϕ the geopotential; T the temperature, c_p the specific heat of dry air at constant pressure; R the dry air gas constant; θ the potential temperature; and ∇ the horizontal der operator on an isobaric surface. The height field (z) is incorporated into this equation through $\phi=gz$, where $g=9.8\ \mathrm{ms}^{-2}$.

The left-hand-side of (1) is a three-dimensional Laplacian of the geopotential tendency, which is approximately proportional to the negative of the height tendency (Holton, 1979, pp. 131–132). The forcing terms on the right-hand-side include the influence of vorticity advection (term A), vertically-differential thermal advection (term B), vertically-differential heating (term C), adiabatic temperature change (term D, see Smith and Tsou, 1988), and friction (term E). To insure ellipticity in (1), the coefficient $(\zeta+f)f/\sigma$ was forced to be positive. Lapse rates were adjusted to be no greater than $9°\mathrm{C\ km}^{-1}$ in order to make σ greater than zero. If the coefficient was still negative after this adjustment, then it was set to the small positive value of $10^{-6}\ \mathrm{kg^2\ m^{-4}\ s^{-4}}$. The relaxation iteration was terminated when the absolute difference between two successive solutions of geopotential tendency was less than $10^{-4}\ \mathrm{m^2\ s^{-3}}$, corresponding to a change in height of 0.4 m in 12 h, for all grid points. Horizontal and vertical derivatives on both sides of the equation were approximated by second-order differencing.

For first-guess and lateral and upper (50 mb) boundary conditions, $\partial\phi/\partial t$ was set equal to zero. The same boundary condition can not be used at the lower boundary because it would compromise our ability to diagnose low-level development. To provide height tendencies at the lower boundary, both for diagnoses at that level and to serve as a lower boundary condition for the solution of (1), an additional diagnostic relationship is needed. For this an extended form of the geostrophic vorticity tendency $(\partial\zeta_g/\partial t)$ equation developed by Zwack and Okossi (1986), known as the Zwack–Okossi (Z–O) development equation, is used. The extended form of the Z–O equation, in analogy to (1), specifies $\partial\zeta_g/\partial t$ as a function of both geostrophic and ageostrophic forcing. Its development proceeds from the hydrostatic equation in the form

$$gz=gz_L+R\int_p^{p_L}\frac{T}{p}\mathrm{d}p, \tag{2}$$

where subscript L refers to a lower boundary pressure level. Operating on (2) with $1/f\ (\nabla^2)$, defining ζ_g as $g/f\ (\nabla^2 z)$, and taking the Eulerian time derivative yields

$$\frac{\partial\zeta_g}{\partial t}=\frac{\partial\zeta_{gL}}{\partial t}+\frac{R}{f}\int_p^{p_L}\nabla^2\frac{\partial T}{\partial t}\frac{\mathrm{d}p}{p}. \tag{3}$$

Applying the vorticity equation for $\partial\zeta_g/\partial t$ and the first law of thermodynamics for $\partial T/\partial t$ yields:

$$\frac{\partial\zeta_{gL}}{\partial t}=-\boldsymbol{V}\cdot\nabla(\zeta+f)+(\zeta+f)\frac{\partial\omega}{\partial p}+\boldsymbol{k}\cdot\nabla\wedge\boldsymbol{F}$$

$$-\frac{R}{f}\int_p^{p_L}\left[\nabla^2(-\boldsymbol{V}\cdot\nabla T)+\nabla^2 S\omega+\nabla^2\frac{\dot{q}}{c_p}\right]\frac{\mathrm{d}p}{p}, \tag{4}$$

where S is $-T/\theta\ \partial\theta/\partial p$ and $\boldsymbol{F}$ the frictional force. Neglect of the tilting, vertical vorticity advection, and ageostrophic vorticity tendency terms in (4) is consistent with the assumptions made in developing (1) (see Tsou, et al., 1987).

The final form of the extended Z–O equation is then obtained by integrating (4) from p_L to the upper boundary P_T, dividing by p_L-p_T, and

noting that the divergence term integrates to a small quantity over this interval to yield

$$\frac{\partial \zeta_{gL}}{\partial t} = \frac{1}{p_L - p_T}\int_{p_T}^{p_L} -\boldsymbol{V}\cdot\nabla(\zeta + f)\,\mathrm{d}p - \frac{1}{p_L - p_T} \tag{A}$$

$$\times \int_{p_T}^{p_L} \frac{R}{f}\int_{p}^{p_L}\left[\nabla^2(-\boldsymbol{V}\cdot\nabla T) + \nabla^2\zeta\omega + \nabla^2\frac{\dot{q}}{c_p}\right]\frac{\mathrm{d}p^*}{p^*}\,\mathrm{d}p \tag{B}\quad(C)\quad(D)$$

$$+\frac{1}{p_L - p_T}\int_{p_T}^{p_L}\boldsymbol{k}\cdot\nabla\wedge\boldsymbol{F}\,\mathrm{d}p. \tag{E}\quad(5)$$

Relaxation of (5) yields the lower boundary height tendency ($\partial z/\partial t$) required in the solution (1). Note that the right-hand-side terms in (5) represent the same physical processes as the corresponding terms in (1). Thus, the contribution of each of the individual terms in (5) to $\partial z_L/\partial t$ can be used as the lower boundary condition for the corresponding term in (1). In this paper the lower boundary is taken to be 950 mb, so chosen because it is above the earth's surface everywhere in the domain of interest but is sufficiently close to the surface to be representative of the surface cyclone development.

Examination of (5) reveals that it is similar to the Petterssen-Sutcliffe development equation (Petterssen, 1956, p. 324). However, whereas the Petterssen-Sutcliffe equation explicitly accounts for upper air forcing only up to the non-divergent level, the Z–O equation includes forcing contributions from all levels above p_L and, thus, explicitly identifies all of the upper air support for surface development. Increases in lower boundary geostrophic vorticity occur whenever any of the terms in (5) yield mass divergence at any level, thus contributing to surface pressure falls. Eq. (5) reveals that this occurs for mechanisms that increase upper air vorticity (e.g., cyclonic vorticity advection) or upper air temperature (e.g., warm air advection or diabatic heating).

Vertical motions were calculated from the omega equation,

$$\nabla^2\sigma\omega + f(f+\zeta)\frac{\partial^2\omega}{\partial p} = f\frac{\partial}{\partial p}\left[\boldsymbol{V}\cdot\nabla(\zeta + f)\right] + \frac{R}{p}\nabla^2(\boldsymbol{V}\cdot\nabla T) - \frac{R}{c_p p}\nabla^2\dot{q} + f\frac{\partial}{\partial p}(\boldsymbol{k}\cdot\nabla\times\boldsymbol{F}). \tag{6}$$

This equation was solved using the same procedure as used for (1). Relaxation iteration was terminated when the absolute difference between two successive solutions of vertical motion was less than 0.01 μbar s^{-1}. Boundary and first-guess values were $\omega = 0$.

The diabatic heating term was calculated for two heating components, latent heat release and boundary layer sensible heating. Latent heat release was divided into two components, stable (grid-scale) and convective (subgrid-scale). The subgrid-scale component was computed using Kuo's (1965, 1974) parameterization scheme with modifications suggested by Edmon and Vincent (1976), Lin and Smith (1979), and Smith et al. (1984). The grid-scale component was determined using procedures described by Krishnamurti and Moxim (1971) and Vincent et al. (1977). Then the total latent heating was modified using GOES IR data in a scheme discussed in Fosdick and Smith (1991). Surface sensible heat flux values used were 6 h forecast values determined from the GLA model and routinely included on GLA analysis tapes. The sensible heating rates required were then proportional to the vertical flux divergence, with flux assumed to vary linearly with pressure from the surface value to zero at 850 mb.

The frictional force was calculated as in Krishnamurti (1968) in which the quantity is evaluated from u and v components of wind, temperature, and a drag coefficient. The drag coefficient was computed from the algorithm used in the GLA GCM (Kalnay et al., 1983) with values assumed to be zero at and above 850 mb.

3. Synoptic discussion

A general discussion of the evolution of the relevant surface and upper-air features from incipient cyclone formation over the Great Lakes on 17 January through block formation on 21 January 1979 is given in Tsou and Smith (1990a). For this paper we will focus on the 24-h period of explosive surface cyclone development from 1200 GMT 18 January through 1200 GMT 19 January (Figs. 1–3). Clearly the analysis resolution dictates that we examine only synoptic-scale processes operative during development of the cyclone system.

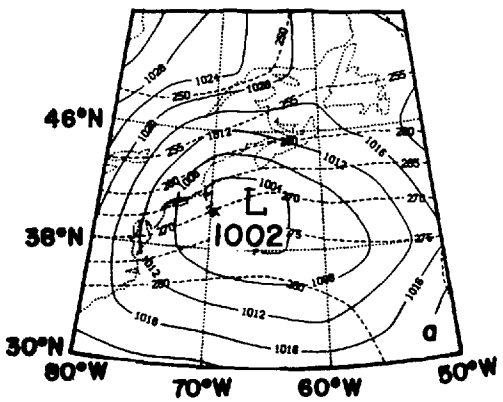

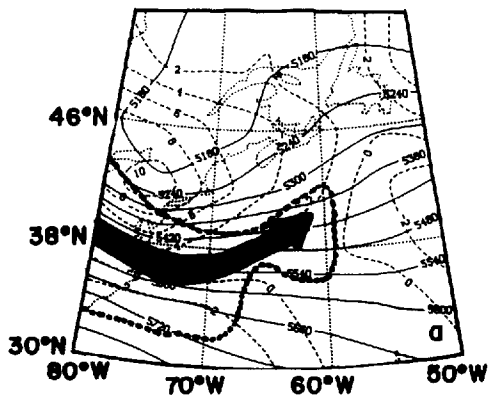

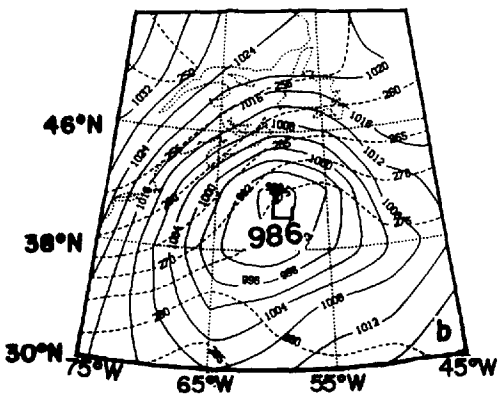

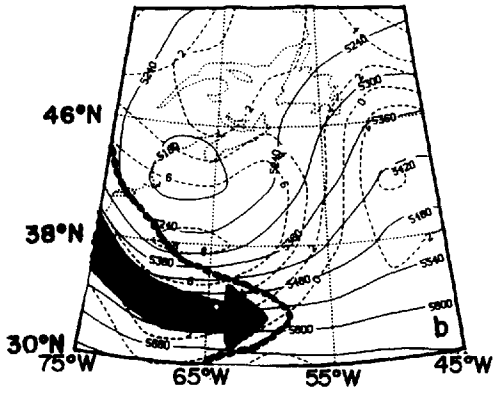

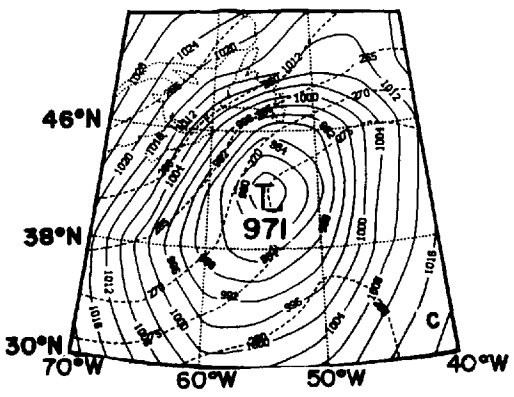

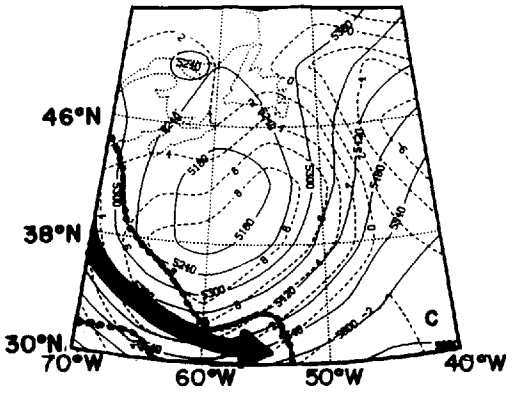

Fig. 1. Sea level pressure (mb, solid) and 850 mb isotherms (°K, dashed) for 1200 GMT 18 January (a), 0000 GMT 19 January (b), and 1200 GMT 19 January 1979 (c).

Fig. 2. 500 mb height (m, solid) and relative vorticity (10^{-5} s^{-1}, dashed) and 300 mb jet axis (heavy arrow) and 50 ms^{-1} isotach (heavy dashed) for the same map times as in Fig. 1.

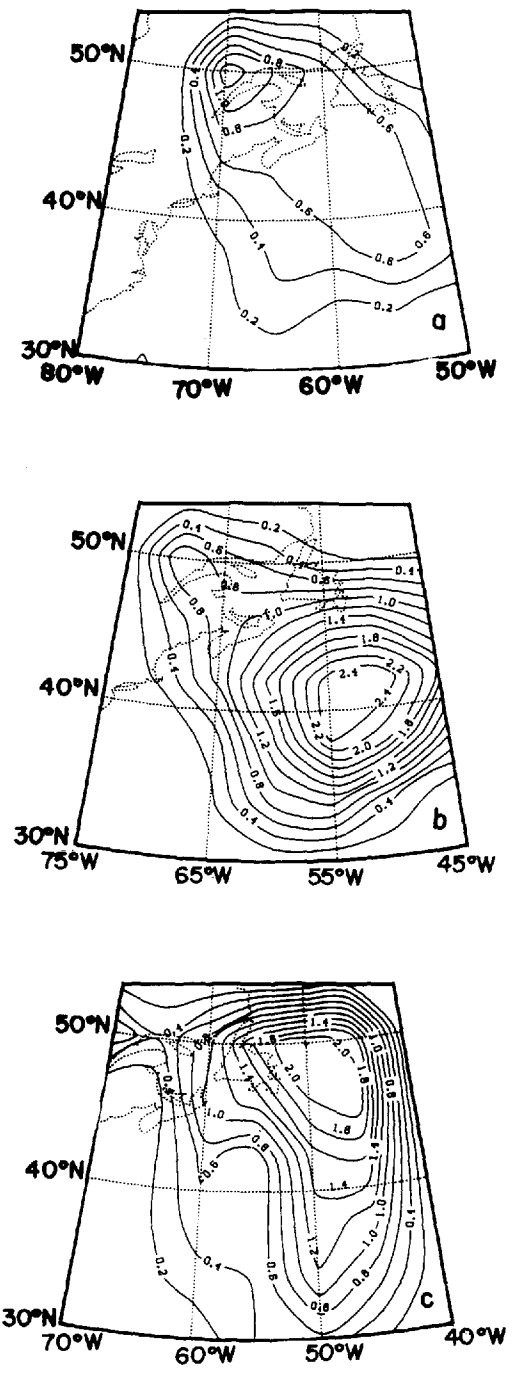

Fig. 3. Precipitation rates (mm h^{-1}) derived from the latent heat release computational scheme (see text) for the same map times as in Fig. 1.

The explosive phase began with a closed low of 1002 mb over the Atlantic Ocean, south of Nova Scotia (Fig. 1). A trough at 500 mb (Fig. 2) was located approximately 550 km upstream from this surface feature, suggesting a highly baroclinic environment. This is confirmed in the 850 mb temperature field (Fig. 1), which shows northward warm air advection over and east and southward cold air advection west of the surface cyclone center, all in a region of relatively strong temperature gradients. Additionally, the surface low was positioned poleward of the exit region of a jet streak at 300 mb (Fig. 2), a condition considered favorable for explosive cyclogenesis (Sanders, 1986; Elsberry and Kirchoffer, 1988). As the surface cyclone moved slowly eastward, it deepened rapidly to 985 mb in the first 12 h and then to its lowest pressure of 971 mb at 1200 GMT on the 19th. The total central pressure decrease of 31 mb corresponds to a deepening rate of 1.7 Bergerons at the cyclone's mean latitude of 42° N. By midway through the explosive phase, a 500 mb low had formed as the surface low remained in the left-front exit region of the 300 mb jet. The westward tilt with height of the system was still evident, though the distance between the upper-level trough and the surface low had decreased. Finally, by the last map time the westward tilt further decreased, and the jet moved well south of the surface cyclone position.

During the cyclone evolution the latent heat release maximum (Fig. 3) progressed from a position north, to the east, and finally to the northeast of the surface cyclone with corresponding precipitation rates in excess of two mm h^{-1} occurring at the second two map times. In addition, it should be noted that throughout the 24 h period the surface cyclone propagated along the mean axis of the Gulf Stream (Lepp, 1973, p. 205).

4. Comparison of model and observed height tendencies

Comparing the calculated height tendency results with observed height changes provides a measure of the extent to which the extended ZO and height tendency equations provide reliable diagnoses of the changes in height which occurred during cyclone development. Observed height changes were determined as the difference in height

at each grid point from 6 h before to 6 h after each map time. Comparative height tendencies were instantaneous values from (1) or (5) at 1200 GMT 18 January and 0000 and 1200 GMT 19 January.

The observed and extended calculations were compared at each level using means of absolute values over all grid points and correlation coefficients between the two. Following the philosophy of Tsou et al. (1987), statistics are presented for the total 24 h period. Both statistics were determined from values within the moving 24° latitude by 30° longitude boxes utilized in the synoptic depictions. These are approximately centered on the surface cyclone position. The absolute means indicate the extent to which the observed and model values are similar in magnitude, while the correlation coefficients measure the pattern comparability between the two fields. Pattern similarity between two fields is indicated by a correlation coefficient near 1, while a dissimilar pattern is indicated by a correlation coefficient near 0.

Table 1 contains the mean absolute observed and extended height tendencies and corresponding correlation coefficients at each level averaged over all three map times. Below 750 mb, the extended height tendency equation overestimated height changes, with a maximum overestimate of 30% at 950 mb. Above 750 mb, the extended equation underestimated height changes with a maximum of about 20% above 500 mb. Correlation coefficients range from 0.84 to 0.94.

Table 1. *Mean absolute observed (OBS) and extended height (EXT) tendencies (m 12 h^{-1}) and correlation coefficients (CC) averaged over the three map times*

Level (mb)	OBS	EXT	CC
200	75.2	53.7	0.84
250	87.0	69.8	0.89
300	89.2	76.6	0.93
350	85.0	77.2	0.93
400	85.8	73.5	0.94
450	79.8	68.6	0.93
500	77.8	63.2	0.92
550	72.4	60.2	0.90
600	69.3	59.4	0.89
650	66.8	59.5	0.88
700	64.5	59.6	0.87
750	62.3	60.2	0.87
800	60.8	63.4	0.87
850	59.7	66.9	0.91
900	59.9	73.2	0.92
950	60.2	79.2	0.92

Discrepancies between observed and calculated tendencies may arise for several reasons. Of course, errors in analyzed data fields and errors induced by the finite differencing procedures can contribute to these discrepancies. In addition, the nonlinear temporal variations in height tendencies that are expected in a rapidly developing system can introduce errors when instantaneous tendencies are compared with difference values calculated over a relatively large (e.g., 12 h) finite time interval. This perhaps explains why the greatest magnitude differences are found at 950 mb, where development is most rapid. Finally, discrepancies may occur because of deficiencies in (1) and (5). These may arise because of terms ignored or because of subsynoptic interactions that could not be detected in the analysis grid. In view of the maximum magnitude error of only 30% and the high correlation coefficients, we are confident that the Z–O and height tendency equations applied in this case provide reliable diagnoses of the cyclone system on the time and space scales dictated by the data set. In addition, this reliability suggests that the synoptic-scale development diagnosed in this study is largely forced by the synoptic-scale processes captured by the analysis grid.

5. Height tendency results

Results of the height tendency calculations are presented at 950 and 500 mb. At both levels the total calculated height tendency field and the individual contributions from terms A, B, D and the latent heating component of term C are presented. At 500 mb the contributions of term E and the sensible heating component of C are not included in the discussion because these are essentially boundary layer processes that had little impact above 850 mb. At 950 mb these two terms, although larger, still remained a factor of four or more less than the other terms and, therefore, did not materially affect the total height tendencies.

5.1. Total calculated height tendencies

950 and 500 mb total calculated height tendencies are displayed for each of the three map times of the explosive development period in

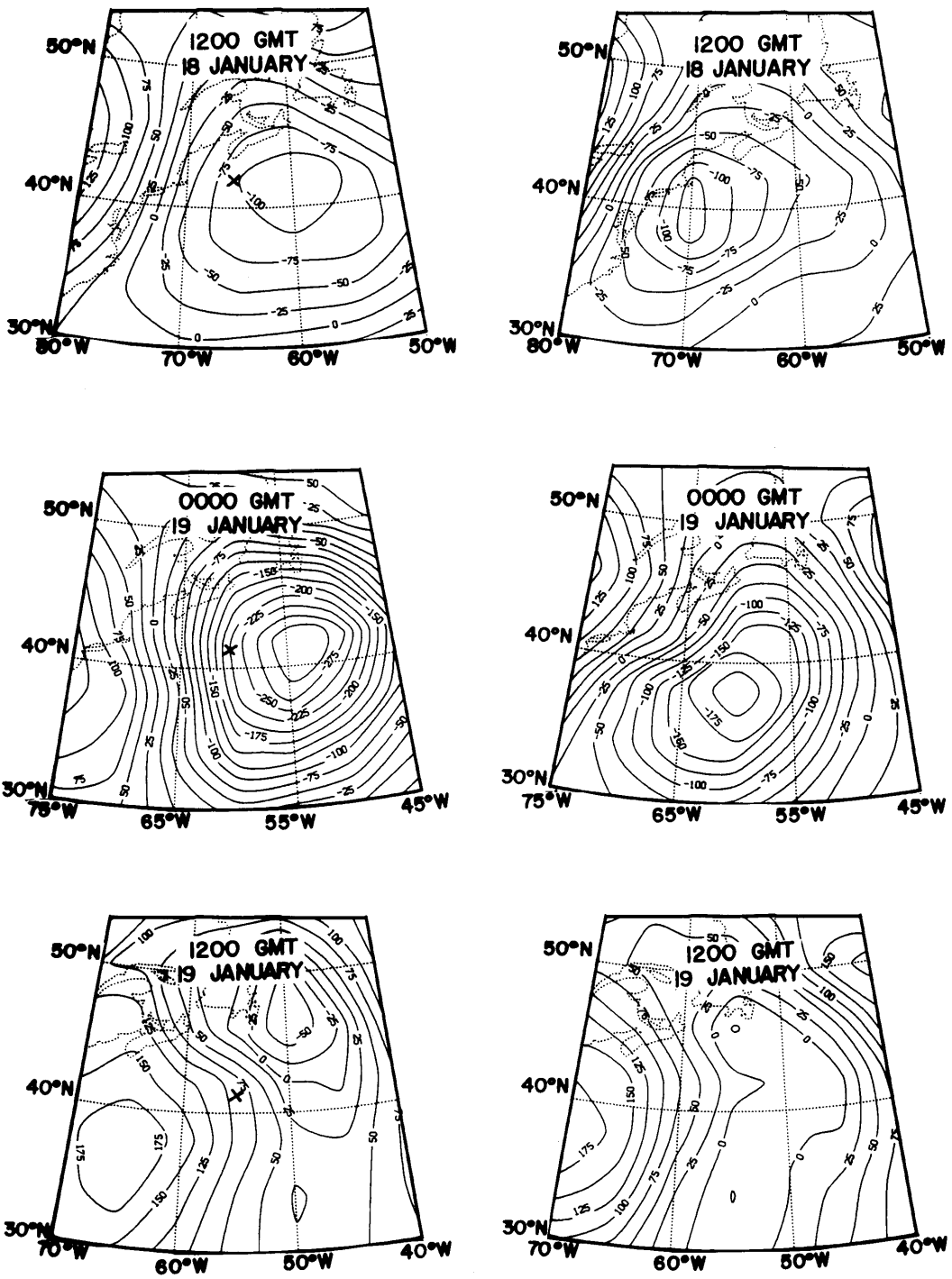

Fig. 4. Total calculated height tendencies (m 12 h^{-1}) determined from (1) or (5). Left column 950 mb, right column 500 mb. X indicates the surface cyclone center.

Fig. 4 (compare with Figs. 1–2). At 1200 GMT 18 January the surface cyclone was positioned within the height fall region just upstream from the height fall maximum, signaling both the subsequent development and eastward propagation of the cyclone. At 500 mb the height fall center was located about 10° longitude west of the 950 mb center, well east of the 500 mb trough (located near the 0 contour) and in the poleward exit region of the 300 mb jet. This suggests rapid trough propagation eastward with little trough development.

By 0000 GMT 19 January the rapid surface cyclone intensification and continued eastward propagation are reflected in the sharply increased 950 mb height falls over and downstream from the cyclone center. At 500 mb the height fall maximum had moved southeastward, consistent with the southeastward propagation of the 500 mb trough and the general upper air wave development that was observed south of 45° latitude and upstream from the surface cyclone.

By the end of the explosive period, the weakened 950 mb height fall maximum had moved northeast of the surface cyclone, which was now positioned well within the height rise region. Similarly, the 500 mb trough was located within the height rise region. At both levels, the height fall regions

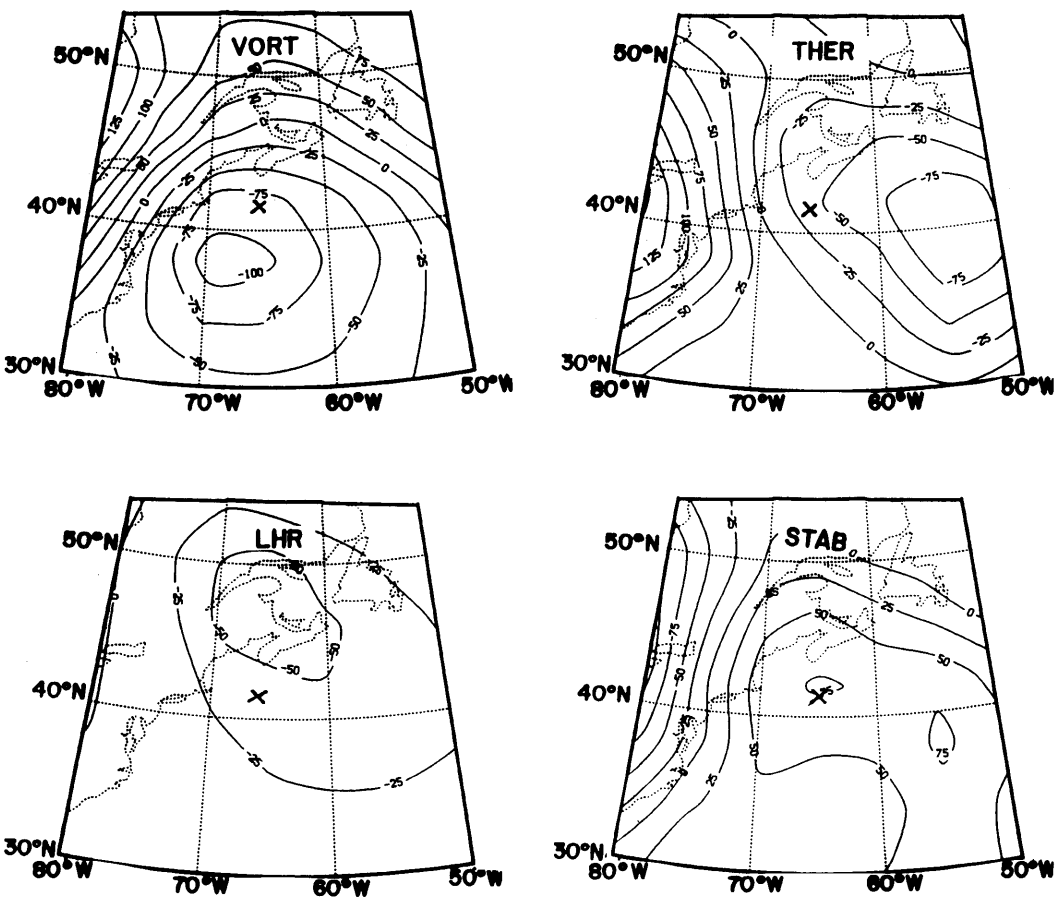

Fig. 5. Height tendencies (m 12 h^{-1}) at 950 mb for 1200 GMT 18 January. X indicates the surface cyclone center. Upper left: Height tendency due to vorticity advection (VORT). Upper right: Height tendency due to temperature advection (THER). Lower left: Height tendency due to latent heat release (LHR). Lower right: Height tendency due to adiabatic temperature change (STAB).

anticipate the northeastward movement of the cyclone features observed over the next 12 h (not shown, see Tsou and Smith, 1990a). During this first 12 h period following explosive development, the surface cyclone central pressure increased by 3 mb, while the 500 mb central height value decreased by 37 m. This latter decrease, occurring despite the fact that the 500 mb center was located at the beginning of the period (1200 GMT 19 January) in an area of height rises, suggests that the height falls must have occurred later in the 12 h period as the upper air cyclone propagated into the height fall region.

5.2. *Individual forcing processes*

The contributions of terms A, B, D, and the latent heating component of C on the right-hand-side of (1) and (5) to the total calculated height tendency at each map time are shown in Figs. 5–10. Because of our primary interest in the surface cyclone and the associated upper air trough, the discussion focuses largely on the height fall regions seen in Fig. 4.

At 1200 GMT 18 January, height falls at both levels (Figs. 5, 6) were primarily the result of cyclonic vorticity advection (VORT) centered downstream from the upper air trough and in the left exit region of the jet. Patterns at both levels were quite similar. Also contributing to height falls, although smaller, were temperature advection (THER) and latent heat release (LHR). At 950 mb the former of these reflects integrated warm air advection above and east of the surface cyclone (see Fig. 1), while the latter reflects the latent heating maximum north of the cyclone (see Fig. 3). At 500 mb, both terms again yielded height

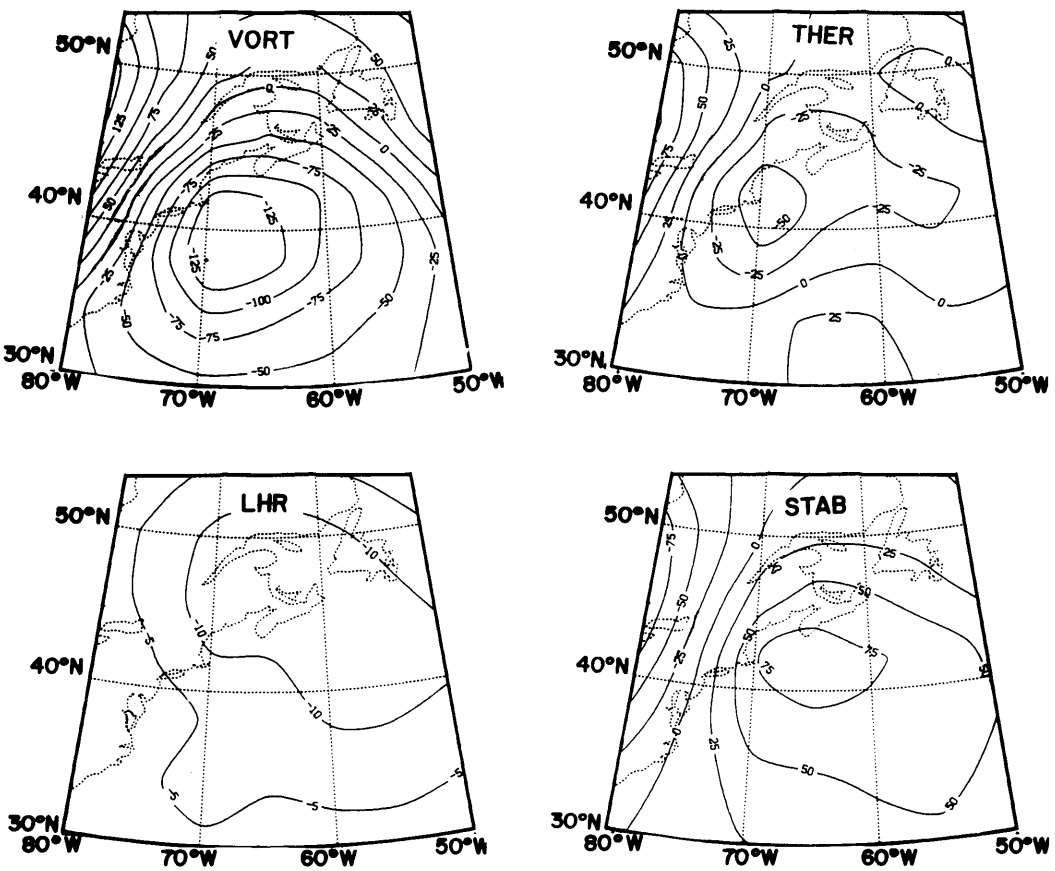

Fig. 6. As in Fig. 5 for 500 mb.

falls. The latent heating maximum was placed similarly to that at 950 mb, but was substantially weaker. However, the 500 mb temperature advection maximum was about 15° longitude west of the 950 mb maximum, the result of cold air advection that decreased with height east of the 500 mb trough. While these thermal mechanisms acted to develop the cyclone, adiabatic cooling in the ascending air (STAB) forced height rises in the cyclone region at both levels. Thus, as previously noted by Petterssen (1956, p. 329) and Tsou, et al. (1987), adiabatic cooling in air that is stable to dry adiabatic processes invariably acts to partially suppress cyclone system development and propagation.

As explosive development ensued (Figs. 7–8), the role of cyclonic vorticity advection showed little change at either level. Rather, the large increase in total calculated height falls at 950 mb seen in Fig. 4 was caused by substantial increases in height falls attributed to warm air advection and latent heat release over and east of the cyclone center. Height falls intensified at 500 mb due to increased lower tropospheric cold air advection west and south of the cyclone center. All of this was once again partially neutralized by adiabatic cooling at both levels.

At the last map time (Figs. 9–10) it is clear that the increase (decrease) in total calculated height rises (falls) that prevailed over the region (Fig. 4) was attributed to vorticity advection, which by now was forcing height rises everywhere in the

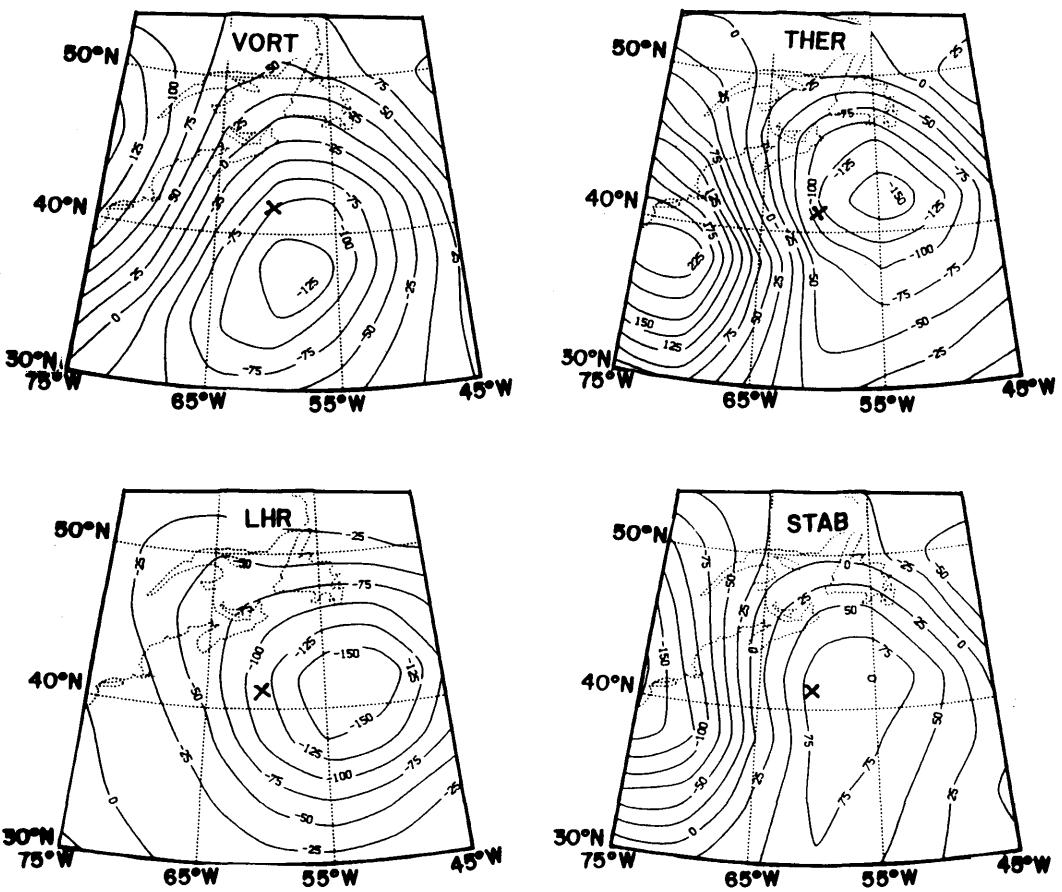

Fig. 7. As in Fig. 5 for 0000 GMT 19 January.

region at 950 mb and nearly so at 500 mb. This occurred despite the fact that from Fig. 2 it is apparent that cyclonic vorticity advection was still in evidence at 500 mb east of about 55° W. This is explained by anticyclonic vorticity advections that prevailed below 600 mb throughout much of the region, thus illustrating the vertical coupling between height changes at one level and forcing processes at other levels that is implied, but often overlooked, in the height tendency equation. Vorticity advections at 500 and 850 mb at this map time are shown in Fig. 11 to exemplify the contrasting patterns. The height falls forced by thermal advection at both levels and by latent heat release at 950 mb showed only minor changes in magnitude from the previous map time as they migrated to a position northeast of the surface cyclone, the direction of subsequent cyclone propagation; while the latent heating influence at 500 mb weakened substantially. Adiabatic temperature changes continued to oppose the thermal advection and latent heating influence at both levels. It should also be noted that, although still small near the cyclone center, a marked increase (to −50 m) in 950 mb sensible heating height falls occurred over the last two map times (not shown) in the wake of the cyclone as cold continental air passed over the warmer ocean surface.

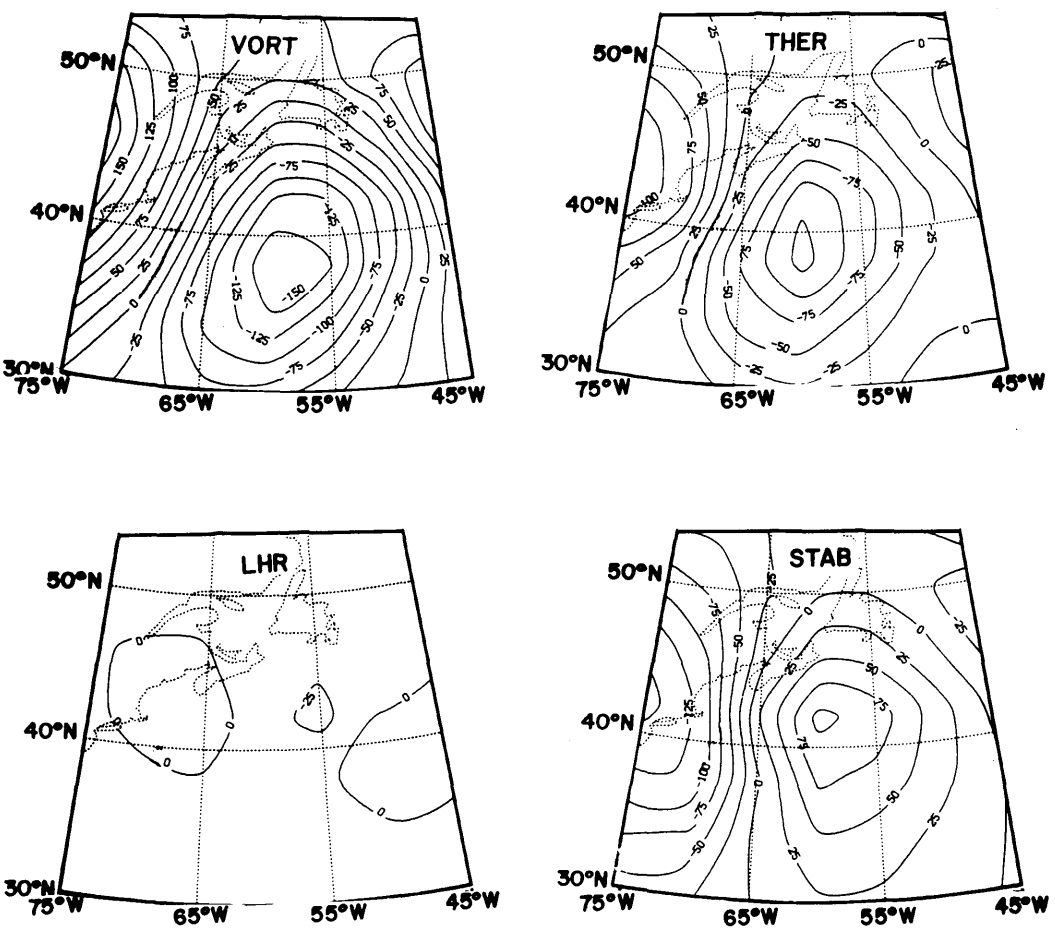

Fig. 8. As in Fig. 6 for 0000 GMT 19 January.

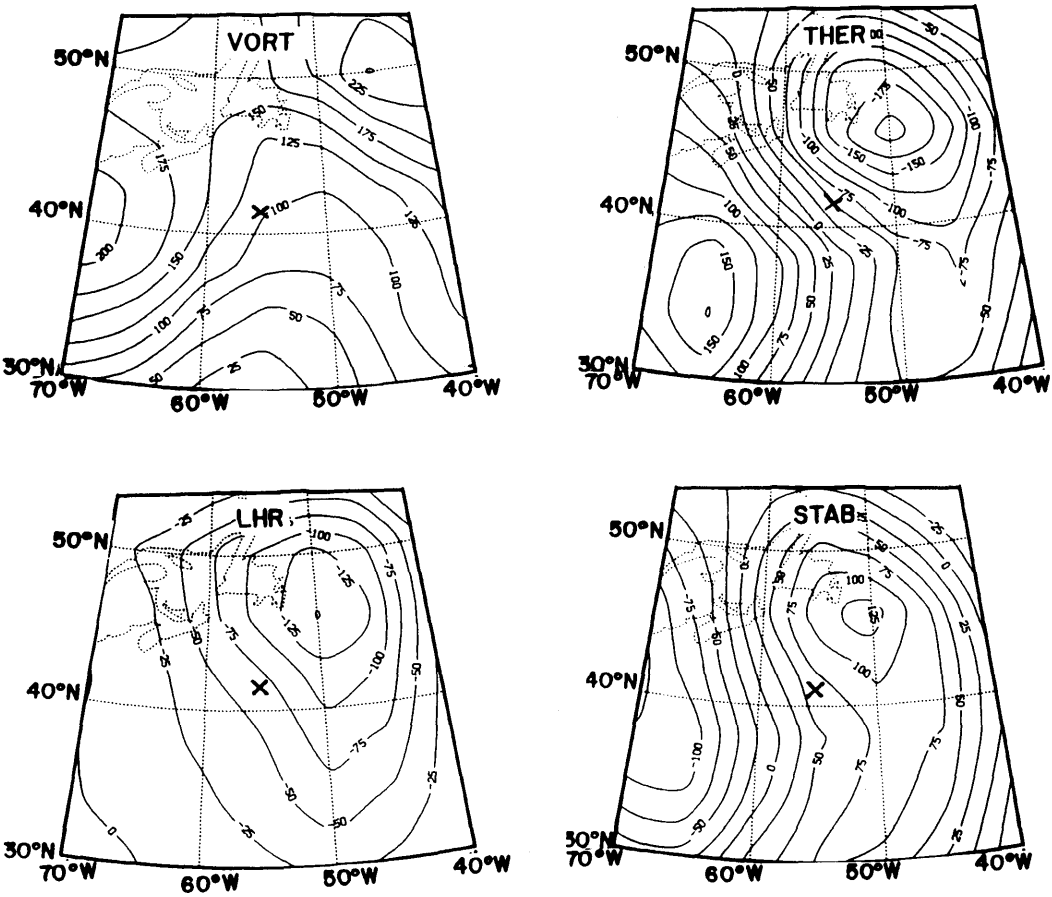

Fig. 9. As in Fig. 5 for 1200 GMT 19 January.

6. Discussion

An explosively-developing cyclone which occurred upstream from a blocking anticyclone over the North Atlantic Ocean has been diagnosed using the extended height tendency and the Zwack–Okossi development equations. The cyclone system evolved from a synoptic-scale wave that propagated from the Great Lakes region eastward over the Atlantic Ocean and developed explosively from 1200 GMT 18 January through 1200 GMT 19 January.

Consistent with the results of Tsou et al. (1987), the cyclone developed in response to cyclonic vorticity advection downstream from the 500 mb trough, warm air advection associated with a strongly baroclinic system, and latent heat release in the cyclone region. The former of these was dominant at the initial time, confirming the importance of this mechanism as suggested by Sanders and Gyakum (1980), Sanders (1986), and MacDonald and Reiter (1988). However, as development continued, vorticity advection decreased its role and eventually forced height rises by the end of the period. At the same time both temperature advection and latent heat release increased sharply, suggesting that the rapid development could be characterized as a transition from a largely dynamically-forced to a thermally-forced system. The importance of warm air

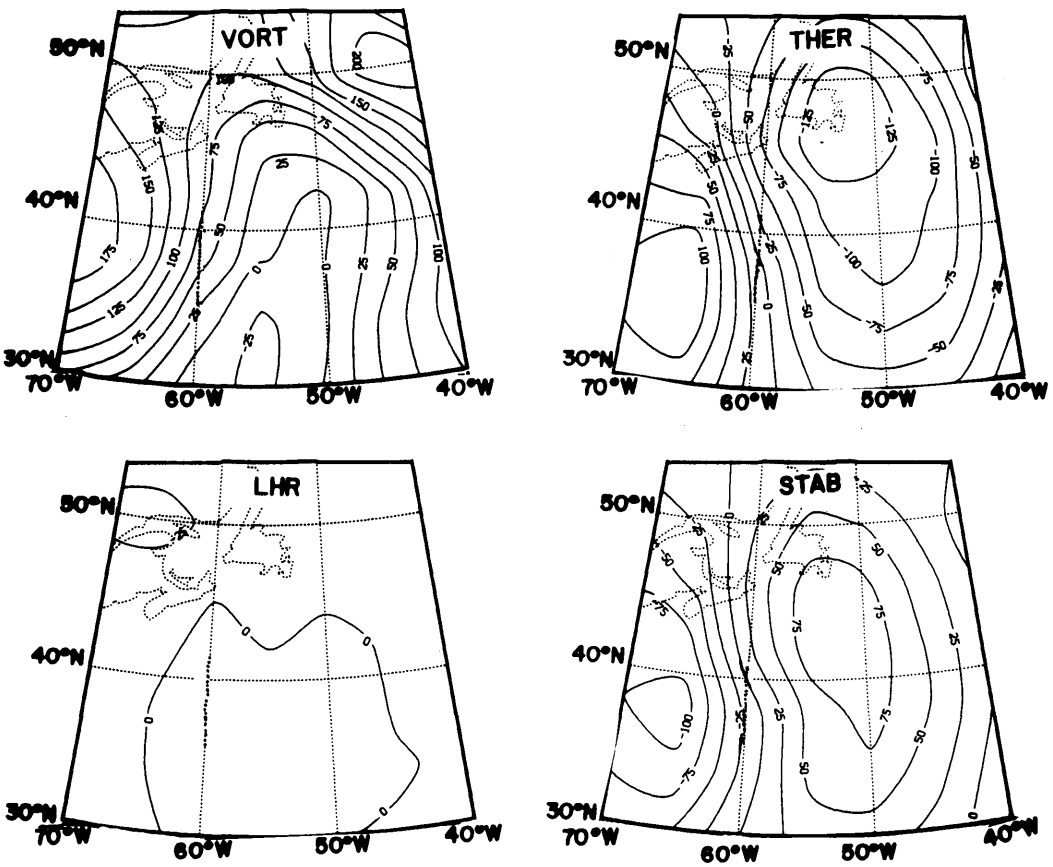

Fig. 10. As in Fig. 6 for 1200 GMT 19 January.

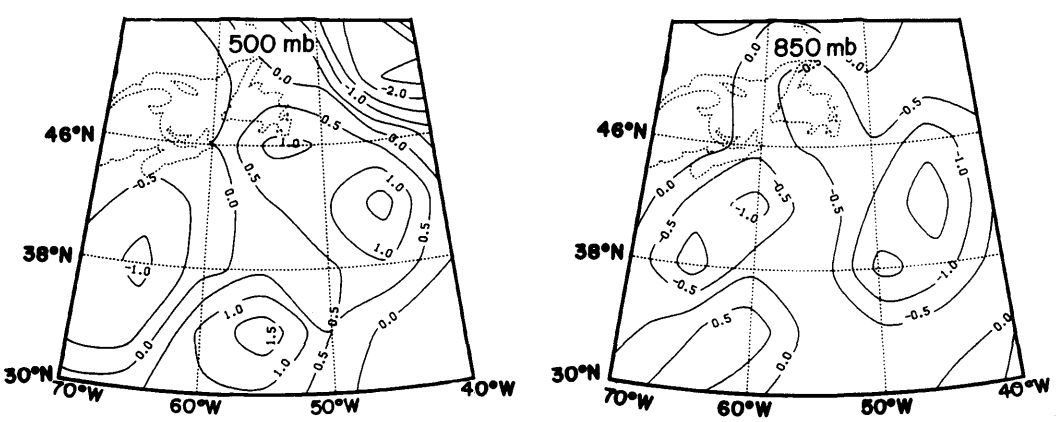

Fig. 11. Absolute vorticity advections (10^{-9} s^{-2}) for 1200 GMT, 19 January at 500 mb (left) and 850 mb (right).

advection in cyclone evolution has been noted recently by Hirschberg and Fritsch (1991) and the significance of latent heat release has been long recognized by many researchers (e.g., Gyakum, 1983; Reed and Albright, 1986; Reed et al., 1988; Kuo and Reed, 1988; and Manobianco, 1989a, b).

Finally, the remaining term, adiabatic cooling, acted to suppress development. A term noted by Petterssen (1956, p. 329) and Tsou, et al. (1987), this quantity, which results from adiabatic cooling of stable (S or $\sigma > 0$) ascending air, was usually comparable to the larger deepening terms and thus exerted a substantial influence on the cyclone's development.

In conclusion, it appears that explosive cyclogenesis resulted from the synergistic interaction of several complementary processes, as hypothesized by Uccellini, et al. (1987). As the cyclone developed, vorticity advection, temperature advection, and latent heat release combined to force strong height falls. However, when the contribution of one of these processes, namely vorticity advection, ended, cyclone development ceased.

7. Acknowledgments

The authors wish to thank Helen Henry for typing the manuscript and Melinda Hunter for preparing the figures. This work was supported by the National Aeronautics and Space Administration under Grant NAG8-764.

REFERENCES

Anthes, R. A., Kuo, Y.-H. and Gyakum, J. R. 1983. Numerical simulations of a case of explosive marine cyclogenesis. *Mon. Wea. Rev. 111*, 1174–1188.

Austin, J. R. 1980. The blocking of middle latitude westerly winds by planetary waves. *Quart. J. Roy. Meteor. Soc. 106*, 327–350.

Baker, W. E. 1983. Objective analysis and assimilation of observational data from FGGE. *Mon. Wea. Rev. 111*, 328–342.

Bergthorsson, P. and Döös, B. 1955. Numerical weather map analysis. *Tellus 7*, 329–340.

Bosart, L. F. and Lin, S. C. 1984. A diagnostic analysis of the President's Day storm of February 1979. *Mon. Wea. Rev. 112*, 2148–2177.

Colucci, S. J. 1985. Explosive cyclogenesis and large-scale circulation changes: Implications for atmospheric blocking. *J. Atmos. Sci. 42*, 2701–2717.

Colucci, S. J. 1987. Comparative diagnosis of blocking versus nonblocking planetary-scale circulation changes during synoptic-scale cyclogenesis. *J. Atmos. Sci. 44*, 124–139.

Cressman, G. 1959. An operational objective analysis system. *Mon. Wea. Rev. 87*, 367–374.

Davis, C. A. and Emanuel, K. A. 1988. Observational evidence for the influence of surface heat fluxes on rapid maritime cyclogenesis. *Mon. Wea. Rev. 116*, 2649–2659.

Edmon, H. J. and Vincent, D. G. 1976. An application of two tropical parameterization schemes of convective latent heat release in middle latitudes. *Mon. Wea. Rev. 104*, 1141–1153.

Elsberry, R. L. and Kirchoffer, P. J. 1988. Upper-level forcing of explosive cyclogenesis over the ocean based on operationally analyzed fields. *Wea. Forecasting 3*, 205–216.

Fosdick, E. G. and Smith, P. J. 1991. Latent heat release in an extratropical cyclone that developed explosively over the southeastern United States. *Mon. Wea. Rev. 119*, 193–207.

Green, J. S. A. 1977. The weather during July 1976: Some dynamic considerations of the drought. *Weather 32*, 120–126.

Gyakum, J. R. 1983. On the evolution of the QE II Storm. Part II: Dynamic and thermodynamic structure. *Mon. Wea. Rev. 111*, 1156–1173.

Gyakum, J. R., Anderson, J. R., Grumm, R. H. and Gruner, E. L. 1989. North Pacific cold season surface cyclone activity: 1975–1983. *Mon. Wea. Rev. 117*, 1141–1155.

Hansen, A. R. and Chen, T.-C. 1982. A spectral energetics analysis of atmospheric blocking. *Mon. Wea. Rev. 110*, 1146–1165.

Hayashi, Y. and Golder, D. G. 1987. Effects of wave-wave and wave-mean flow interactions on the growth and maintenance of transient planetary waves in the presence of a mean thermal restoring force. *J. Atmos. Sci. 44*, 3392–3401.

Hirschberg, P. A. and Fritsch, M. G. 1991. Tropopause undulations and the development of extratropical cyclones. Part II: Diagnostic analysis and conceptual model. *Mon. Wea. Rev. 119*, 518–550.

Holton, J. R. 1979. *An introduction to dynamic meteorology* 2nd edition. Academic Press, 391 pp.

Illari, L. 1984. A diagnostic study of the potential vorticity in a warm blocking anticyclone. *J. Atmos. Sci. 41*, 3518–3526.

Kalnay, E., Balgovind, R., Chao, W., Edelmann, D., Pfaendtner, J., Takacs, L. and Takano, K. 1983. *Documentation of the GLAS fourth-order general circulation model.* Vol. I NASA Tech. Memo 86–64, Goddard Space Flight Center, Greenbelt, MD.

Kalnay-Rivas, E., Bayliss, A. and Storch, J. 1977. The 4th order GISS model of the global atmosphere. *Beitr. Phys. Atmos. 50*, 299–311.

Kalnay-Rivas, E. and Hoitsma, D. 1979. The effect of accuracy, conservation and filtering on numerical weather forecasting. *Preprints 4th Conf. Numerical Weather Prediction*, Silver Spring, MD, Amer. Meteor. Soc., 302–312.

Krishnamurti, T. N. 1968. A diagnostic balance model for studies of weather systems of low and high latitudes, Rossby number less than 1. *Mon. Wea. Rev. 96*, 197–207.

Krishnamurti, T. N. and Moxim, W. J. 1971. On parameterization of convective and nonconvective latent heat release. *J. App. Meteor. 10*, 3–13.

Kuo, H. L. 1965. On formation and intensification of tropical cyclones through latent heat release by cumulus convection. *J. Atmos. Sci. 22*, 40–63.

Kuo, H. L. 1974. Further studies of the parameterization of the influence of cumulus convection on a large-scale flow. *J. Atmos. Sci. 31*, 1232–1240.

Kuo, Y.-H. and Reed, R. J. 1988. Numerical simulation of an explosively deepening cyclone in the eastern Pacific. *Mon. Wea. Rev. 116*, 2081–2105.

Lepp, H. 1973. *Dynamic earth.* McGraw-Hill, New York, 485 pp.

Lin, S. C. and Smith, P. J. 1979. Diabatic heating and generation of available potential energy in a tornado-producing extratropical cyclone. *Mon. Wea. Rev. 107*, 1169–1183.

MacDonald, B. C. and Reiter, E. R. 1988. Explosive cyclogenesis over the eastern United States. *Mon. Wea. Rev. 116*, 1568–1586.

Manobianco, J. 1989a. Explosive east coast cyclogenesis over the west-central North Atlantic Ocean: A composite study derived from ECMWF operational analyses. *Mon. Wea. Rev. 117*, 2365–2383.

Manobianco, J. 1989b. Explosive east coast cyclogenesis: Numerical experimentation and model-based diagnostics. *Mon. Wea. Rev. 117*, 2384–2405.

Mullen, S. L. 1987. Transient eddy forcing of blocking flows. *J. Atmos. Sci. 44*, 3–22.

Nuss, W. A. and Anthes, R. A. 1987. A numerical investigation of low-level processes in rapid cyclogenesis. *Mon. Wea. Rev. 115*, 2728–2743.

Petterssen, S. 1956. *Weather analysis and forecasting, vol.* I, 2nd edition. McGraw-Hill, New York, 428 pp.

Reed, R. J. and Albright, M. D. 1986. A case study of explosive cyclogenesis in the eastern Pacific. *Mon. Wea. Rev. 114*, 2297–2319.

Reed, R. J., Simmons, A. J., Albright, M. D. and Unden, P. 1988. The role of latent heat release in explosive cyclogenesis: Three examples based on ECMWF operational forecasts. *Wea. Forecasting 3*, 217–229.

Roebber, P. J. 1989. The role of surface heat and moisture fluxes associated with large-scale ocean current meanders in maritime cyclogenesis. *Mon. Wea. Rev. 117*, 1676–1694.

Sanders, F. 1986. Explosive cyclogenesis in the west-central north Atlantic Ocean, 1981–84. Part I: Composite structure and mean behavior. *Mon. Wea. Rev. 114*, 1781–1794.

Sanders, F. and Gyakum, J. R. 1980. Synoptic-dynamic climatology of the "bomb". *Mon. Wea. Rev. 108*, 1589–1606.

Shutts, G. J. 1983. The propagation of eddies in diffluent jet streams. Eddy vorticity forcing of blocking flow fields. *Quart. J. Roy. Meteor. Soc. 109*, 737–761.

Smith, P. J., Dare, P. M. and Lin, S.-J. 1984. The impact of latent heat release on synoptic-scale vertical motions and the development of an extratropical cyclone system. *Mon. Wea. Rev. 112*, 2421–2430.

Smith, P. J. and Tsou, C.-H. 1988. Static stability variations during the development of an intense extratropical cyclone. *Mon. Wea. Rev. 116*, 1245–1250.

Tsou, C.-H. and Smith, P. J. 1990a. The role of synoptic/planetary-scale interactions during the development of a blocking anticyclone. *Tellus 42A*, 174–193.

Tsou, C.-H. and Smith, P. J. 1990b. The importance of non-quasigeostrophic forcing during the development of a blocking anticylone. *Tellus 42A*, 328–342.

Tsou, C.-H., Smith, P. J. and Pauley, P. M. 1987. A comparison of adiabatic and diabatic forcing in an intense extratropical cyclone system. *Mon. Wea. Rev. 115*, 763–785.

Uccellini, L. W., Keyser, D., Brill, K. F. and Wash, C. H. 1985. President's Day cyclone of 18–19 February 1979: Influence of upstream trough amplification and associated tropopause folding on rapid cyclogenesis. *Mon. Wea. Rev. 113*, 962–988.

Uccellini, L. W., Petersen, R. A., Brill, K. F., Kocin, P. J., and Tuccillo, J. J. 1987. Synergistic interactions between an upper level jet streak and diabatic processes that influence the development of a low-level jet and a secondary coastal cyclone. *Mon. Wea. Rev. 115*, 2227–2261.

Vincent, D. G., Pant, G. B. and Edmon, H. J. 1977. Generation of available potential energy of an extratropical cyclone system. *Mon. Wea. Rev. 105*, 1252–1265.

Wash, C. H., Peak, J. E., Calland, W. E. and Cook, W. A. 1988. Diagnostic study of explosive cyclogenesis during FGGE. *Mon. Wea. Rev. 116*, 431–451.

Zwack, P. and Okossi, B. 1986. A new method for solving the quasi-geostrophic omega equation by incorporating surface pressure tendency data. *Mon. Wea. Rev. 114*, 655–666.